Title

Glass Transition Temperature and Ion Binding Determine Conductivity and Lithium-Ion Transport in Polymer Electrolytes

Authors

Schauser, Nicole S
Nikolaev, Andrei
Richardson, Peter M
et al.

Publication Date

2020-12-22

DOI

10.1021/acsmacrolett.0c00788

Peer reviewed

The Glass Transition Temperature and Ion Binding Determine Conductivity and Lithium–Ion Transport in Polymer Electrolytes

Nicole S. Schauser,[†,‡,¶,⊥] Andrei Nikolaev,[§,¶,⊥] Peter M. Richardson,[‡,¶] Shuyi Xie,[‡,¶] Keith Johnson,[†,‡] Ethan M. Susca,[‡] Hengbin Wang,[¶] Ram Seshadri,[‡,†,§] Raphaële J. Clément,[‡,†,¶] Javier Read de Alaniz,[§] and Rachel A. Segalman[*,‡,†,∥,¶]

†*Materials Department, University of California, Santa Barbara, California 93106, United States*
‡*Materials Research Laboratory, University of California, Santa Barbara, California 93106, United States*
¶*Mitsubishi Chemical Center for Advanced Materials*
University of California, Santa Barbara, California 93106, United States
§*Department of Chemistry and Biochemistry*
University of California, Santa Barbara, California 93106, United States
∥*Department of Chemical Engineering, University of California, Santa Barbara, California 93106, United States*
⊥*Contributed equally to this work*

Received December 15, 2020; E-mail: segalman@ucsb.edu

Abstract:

Polymer electrolytes with high Li^+–ion conductivity provide a route towards improved safety and performance of Li^+–ion batteries. However, most polymer electrolytes suffer from low ionic conduction, and an even lower Li^+ ion contribution to the conductivity (the transport number, t_+), with the anion typically transporting over 80% of the charge. Here, we show that subtle and potentially undetected associations within a polymer electrolyte can entrain both the anion and the cation. When removed, the conductivity performance of the electrolyte can be improved by almost two orders of magnitude. Importantly, while some of this improvement can be attributed to a decreased glass transition temperature T_g, the removal of the amide functional group reduces interactions between the backbone and Li^+ cations, doubling the Li^+ t_+ to 0.43, as measured using pulsed-field-gradient NMR. This work highlights the importance of strategic synthetic design and emphasizes the dual role of T_g and ion binding for the development of polymer electrolytes with increased total ionic conductivity and the Li^+ ion contribution to it.

High energy density Li^+–ion batteries have revolutionized both consumer electronics and electrified transportation.[1] However, current Li-ion technology based on organic liquid electrolytes suffers from low chemical, thermal and mechanical stability, leading to substantial safety concerns.[1–3] Ion-conducting polymers form chemically stable, easily processable and mechanically robust films and could lead to safer and higher performing batteries.[2–4] Currently, however, polymer electrolytes lack the ionic conductivity performance required for their use in commercial applications.[5] Significant effort has focused on polymers based on poly(ethylene oxide), and while a few polymers have reached ionic conductivities on the order of 10^{-4} S cm^{-1},[6] some studies suggest that the Li^+ ion only contributes a small fraction of this conductivity (cation transport number, t_+).[7] In fact, both liquid and polymer electrolytes usually transport anions better than cations, with t_+ ranging from -4.5 to 0.2 for standard salt-in-polymer electrolytes,[7–10] while some polymer-in-salt polycarbonate electrolytes have pushed t_+ as high as 0.66.[11] This cation entrapment is a result of the specific solvation mechanism of most polymer electrolytes wherein it is challenging to separate the solvation and conduction functions. Thus, finding different polymer classes that enable tuning of polymer-ion interactions for both high ionic conductivity and high t_+ is critical for further advancement in polymer electrolyte performance.

Metal-ligand coordination polymers enable tunable dynamic interactions between cations and ligands tethered to a polymer backbone[12–15] and promote salt dissolution even with low polarity polymer backbones,[16] providing a large library of polymers for optimizing conductivity performance.[10,16,17] Ion conduction in polymer electrolytes is achieved through the dissolution of a metallic salt and subsequent transport of the metal cation and organic anion.[18–20] Polymer electrolytes must therefore contain solvating groups that interact with ions (typically the cation) to stabilize ionic species but still allow for ion mobility.[10,11,21] Careful choice of the solvating group is warranted, as a strong tradeoff exists between good solvation resulting in effective salt dissolution and strong cation-polymer binding leading to low t_+. We have previously demonstrated the dynamic metal-ligand coordination of imidazole-containing polymers towards lithium and other metal ions, suggesting this class of materials satisfies these requirements.[10,16,17]

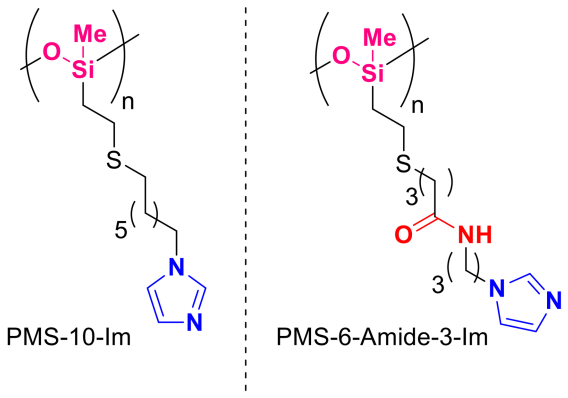

Figure 1. Structure comparison between the amide-free (PMS-10-Im) and the amide-containing (PMS-6-Amide-3-Im) polymers. Both polymers are based on a low T_g siloxane backbone and grafted imidazole ligand, but differ in their linker chemistry.

In this communication, we show how rational polymer de-

sign can result in dramatic improvements in both total ionic conductivity and Li^+ t_+. We functionalize a low T_g siloxane polymer backbone with an imidazole-based ligand, but change the linker identity from a more easily synthesized amide-containing linker (forming PMS-6-Amide-3-Im) to an aliphatic chain (forming PMS-10-Im, figure 1). This improves room temperature ionic conductivity by two orders of magnitude, and Li^+ t_+ by a factor of two due to the removal of the hydrogen bonding and Li^+-coordinating amide group. This work highlights the role of both intended and unintended ion binding sites within a polymer in controlling both T_g and ion mobility.

The PMS-10-Im polymer was designed to reduce polymer T_g and eliminate unwanted ion-polymer interactions through the removal of unnecessary polar functional groups. The ionic conductivity of most polymer electrolytes is governed by Vogel-Fulcher-Tamman temperature dependence, where free volume and segmental dynamics (as measured by the glass transition temperature, T_g) strongly affect ion mobility.[22–24] Thus, low T_g polymer electrolytes are favorable for higher conductivity performance. In our previous work, we showed that backbone polarity is unimportant for ion conductivity performance, emphasizing that backbone choice should focus on T_g rather than polarity.[16] Therefore, poly(methylsiloxane) was chosen for this study because it is non-coordinating and possesses low T_g.[6,16] While the siloxane backbone itself shows low T_g, the T_g increases by over 100 °C upon functionalization with the first-generation imidazole ligand.[16] We hypothesize that the hydrogen-bonding capability of the amide functional group might be one of the factors contributing substantially to this increase.

Scheme 1. Synthesis plan for the amide-free imidazole-containing polymer.

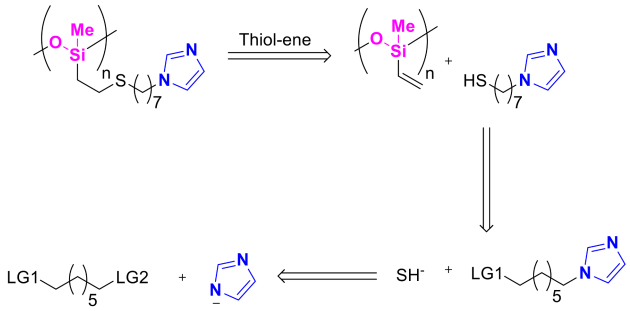

To construct an amide-free imidazole-containing polymer a modular synthetic approach was envisioned (Scheme 1). Attaching an amide-free imidazole-containing side-chain onto the poly(methylsiloxane) backbone can be readily accomplished using an alkene hydrothiolation reaction (thiol-ene) between poly(vinylmethylsiloxane) (PVMS) and a thiol-alkyl-imidazole.[17] We envisioned that synthesis of a thiol-alkyl-imidazole side-chain could be achieved through sequential substitution reactions. Using an alkyl chain bearing a leaving group (LG1 and LG2 in Scheme 1) at each terminal carbon allows for two sequential substitution reactions, first with an imidazole then with an SH^- source.

The amide-free imidazole-grafted siloxane polymer (PMS-10-Im) was compared to the previously reported[16] amide-containing version (PMS-6-Amide-3-Im) to identify whether the amide group enhanced or decreased Li^+–ion transport. The two-step synthesis of PMS-6-Amide-3-Im polymer started with an addition reaction between γ-thiobutyrolactone and 1-(3-aminopropyl)imidazole to yield the corresponding thiol-

Scheme 2. Synthesis of the amide and amide-free imidazole-containing polymers.

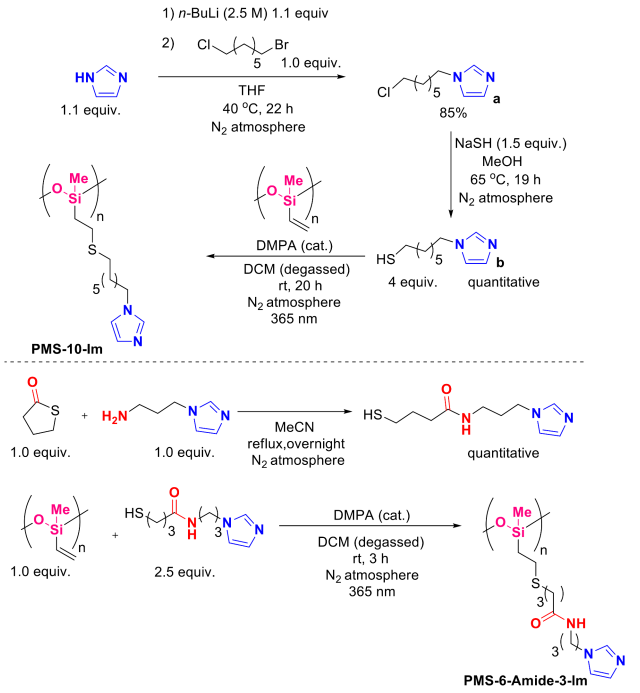

containing product. In the next step, this thiol-containing side chain was readily introduced onto PVMS through hydrothiolation reaction under continuous irradiation with 365 nm light. The three-step synthesis of PMS-10-Im began with a substitution reaction between 1-lithio-1H-imidazole (generated in situ from imidazole and *n*-BuLi) and 1-bromo-7-chloroheptane to yield the corresponding product **a** (Scheme 2). In the second step, a substitution reaction between **a** and sodium hydrogen sulfide (NaSH) lead to the corresponding thiol product **b** (Scheme 2). Utilizing light-driven hydrothiolation reaction between thiol **b** and PVMS allows access to the amide-free imidazole-containing target polymer PMS-10-Im (Scheme 2). The successful synthesis of an amide-free imidazole grafted polymer resulted in a decrease in polymer T_g from −8 °C to −44 °C (Table S2), suggesting the amide was indeed detrimentally increasing T_g.

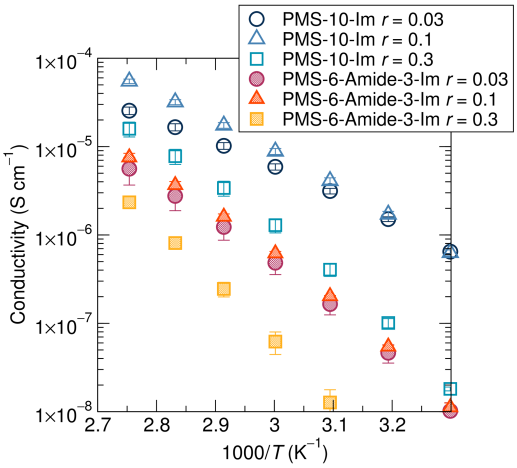

Figure 2. Ionic conductivity as a function of temperature, showing about two orders of magnitude change in room-temperature conductivity associated with the presence or absence of the amide functional group.

The total ionic conductivity performance of these two polymers mixed with lithium bis(trifluoromethanesulfonly)imide (LiTFSI) salt was compared using impedance spectroscopy. Figure 2 shows a 56–63× improvement in the ionic conductivity of the amide-free polymer electrolyte at room temperature, with the improvement decreasing to just over half an order of magnitude at 90 °C, slightly dependent on salt concentration (see Table S3). This is a dramatic increase in conductivity solely driven by the removal of the polar and hydrogen-bonding amide functional group from the side-chains of the polymer electrolyte. This confirms the subtle role played by functional groups even when they constitute only a small part of the overall polymer chemistry and suggests paths to enhance the total conductivity performance.

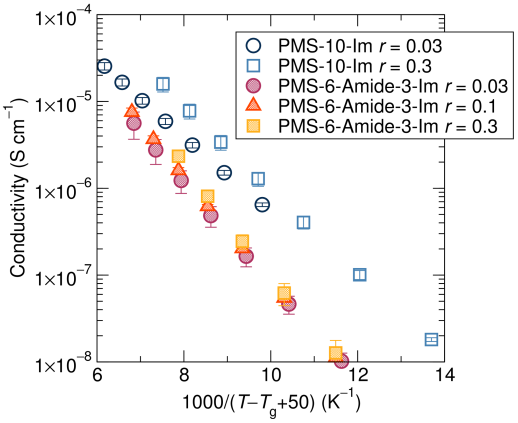

Figure 3. T_g-normalized ionic conductivity still shows over a magnitude improvement in the conductivity through the removal of the amide functional group, suggesting that the conductivity increase is not solely governed by T_g effects.

The curved nature of the conductivity data plotted in an Arrhenius fashion suggests the influence of segmental dynamics on conductivity. To ascertain the extent to which T_g plays a role in conductivity improvement, the conductivity data can be normalized by T_g. The removal of the amide functional group, PMS-10-Im, still results in a 10-fold increase in conductivity over PMS-6-Amide-3-Im after normalization by the T_g of each sample (figure 3). Normalization in a T_g/T representation is also shown in the SI, revealing similar trends. These T_g-normalized representations highlight that T_g only accounts for a little less than half of the conductivity improvement of the amide-free polymer. Importantly, this suggests that the amide is also participating in ion solvation and binding.

Total conductivity as measured using impedance spectroscopy does not provide information on which ions contribute to the ionic conductivity. It is therefore unclear from these measurements alone whether the amide interacts more strongly with the Li^+ cation or $TFSI^-$ anion. To probe individual ion mobilities in each electrolyte more closely, these polymers were studied further using pulsed-field-gradient (PFG) and NMR relaxometry.

PFG experiments reveal an increase in the Li^+ t_+ from 0.23 for the amide-containing polymer to 0.46 for the amide-free polymer at 72.7 °C (Table 1). This arises from a clear increase in the Li^+ diffusion constant for the amide-free polymer compared to the amide-containing polymer. Interestingly, the amide-free polymer also shows a decrease in $TFSI^-$ diffusion, possibly due to increased ion-ion interactions from a higher salt concentration.

Li^+ t_+ measurements confirm that the amide group slows down the dynamics of the Li^+ ions, which is consistent with the conductivity data. Unlike the $TFSI^-$ ions, the Li^+ ions are expected to interact with the polymer side-chains, specifically, with the nitrogen site of the imidazole [10,16] but also, as shown here, with the amide site. Therefore, the observed increase in conductivity through the removal of the amide group can be attributed to a combination of decreased T_g and selective enhancement of the Li^+ dynamics.

PFG NMR also suggests that the fraction of ions not participating in the conduction process is roughly equal for the two polymers. This fraction is determined by comparing the measured conductivity to the conductivity calculated using the self-diffusion constants (D_+ and D_-) determined from PFG NMR (Table 1, calculations in SI). Here, the measured conductivity is about half of that calculated from PFG NMR, which does not account for any neutral pairs or clusters that do not contribute to net charge transport. While it is not possible to determine whether the loss of ions corresponds to the loss of Li^+, $TFSI^-$ ions or a combination of both, since the fraction of ions that do not participate in the conduction process is similar for the two polymers, it is fair to assume that the observed increase in transport number is reliable. The diffusion constants, transport numbers, calculated conductivity arising from the cation (σ_+), anion (σ_-) and total calculated and measured conductivities are summarized in Table 1 for both polymers.

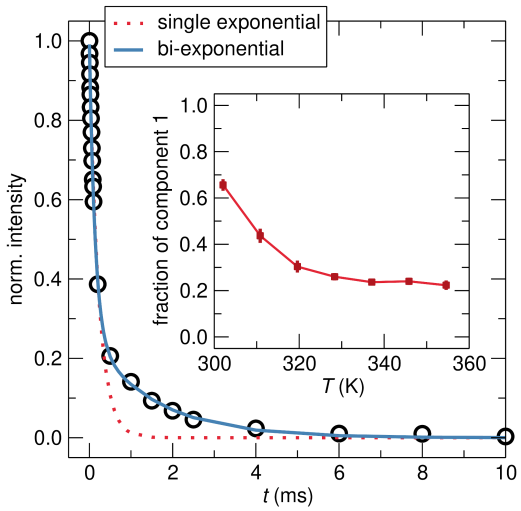

Figure 4. $T_{1\rho}$ decay curve measured at 55.2 °C for amide-free polymer requires a two component fit, highlighting the existence of at least two Li environments. Temperature dependence of component 1 contribution is shown in the inset.

Finally, NMR spin-lattice relaxation time measurements in the rotating frame of reference ($T_{1\rho}$) were used to distinguish between ion environments with significant differences in dynamics. $T_{1\rho}$ results reveal at least two distinct Li environments in the two polymers (figure 4). Li^+ ions in the polymer matrix thus exist in a faster-diffusing and slower-diffusing environment, and the measured D_+ self-diffusion constants shown in Table 1 are a weighted average over these two sites. Since these two Li^+ environments are present in both the amide-free and amide-containing polymers, they may correspond to Li^+ bound to the imidazole (slower component) and 'free' Li^+ (faster component), yet the exact nature of the 'free' Li^+ cannot be determined from these results. Notably, $T_{1\rho}$ relaxation measurements enable the determination of not only the $T_{1\rho}$ for each Li^+ environment, but also the distribution of Li^+ species over the two sites. The contribution from com-

Table 1. Li^+ (D_+) and $TFSI^-$ (D_-) self-diffusion constants, Li^+ transport numbers, calculated conductivity arising from the Li^+ (σ_+) and $TFSI^-$ (σ_-), as well as the total calculated conductivity (σ_{total}) and interpolated measured conductivity as a function of temperature for an amide-free polymer with Li:monomer = 0.3 (0.1 in SI) and amide-containing polymer with Li:monomer = 0.1.

	Diffusion Constants ($\times 10^{-13}\,m^2\,s^{-1}$)			Conductivity ($\times 10^{-5}\,S\,cm^{-1}$)			
Temp (°C)	D_+	D_-	t^+ (%)	σ_+	σ_-	σ_{total}	$\sigma_{measured}$
Amide-Free							
72.7	1.7	2.0	0.46	0.57	0.68	1.3	0.6
81.4	3.1	4.2	0.42	1.0	1.4	2.4	1.2
Amide-Containing							
72.7	1.0	3.3	0.23	0.11	0.34	0.44	0.2
81.4	1.9	6.2	0.23	0.19	0.62	0.82	0.5

ponent 1 (the faster diffusing of the two sites, determined from the relative activation energies, see SI) is observed to decrease with increasing temperature (figure 4, inset). A detailed analysis of the relaxation can be found in the supporting information.

In conclusion, we have shown that the ionic conductivity of polymer electrolytes can be improved by orders of magnitude through rational polymer design. The removal of the hydrogen-bonding and Li^+-coordinating amide functionality in a metal-ligand coordination polymer enables a 100-fold increase in room-temperature total ionic conductivity and a doubling of the Li^+ transport number. These results emphasize the large gains that can be made in electrolyte performance through the targeted removal of detrimental functional groups. Further improvements in electrolytes based on metal-ligand coordination can be expected through careful choice of ligand moiety, as heterocycles offer tunability of their electronic and steric properties that can readily be exploited in structure-function relationship studies in the future.

Supporting Information Available: Characterization including SEC traces, NMR integrations, DSC traces, conductivity as a function of temperature, further NMR results.

Acknowledgement This work was supported by the MRSEC Program of the National Science Foundation under Award No. DMR 1720256 (IRG-2). N.S.S gratefully acknowledges the Fannie and John Hertz Foundation and the National Science Foundation Graduate Research Fellowship Program under Grant 1650114. Any opinions, findings, and conclusions or recommendations expressed in this material are those of the authors and do not necessarily reflect the views of the National Science Foundation.

References

(1) Tarascon, J.-M.; Armand, M. *Issues and challenges facing rechargeable lithium batteries*; 2001.
(2) Quartarone, E.; Mustarelli, P. Electrolytes for solid-state lithium rechargeable batteries: Recent advances and perspectives. 2011.
(3) Manthiram, A.; Yu, X.; Wang, S. Lithium battery chemistries enabled by solid-state electrolytes. 2017.
(4) Hallinan, D. T.; Balsara, N. P. Polymer Electrolytes. *Annu. Rev. Mater. Res* **2013**, *43*, 503–525.
(5) Goodenough, J. B.; Kim, Y. Challenges for Rechargeable Li Batteries. *Chem. Mater* **2010**, *22*, 587–603.
(6) Hooper, R.; Lyons, L. J.; Mapes, M. K.; Schumacher, D.; Moline, D. A.; West, R. Highly Conductive Siloxane Polymers. *Macromolecules* **2001**, *34*, 931–936.
(7) Pesko, D. M.; Timachova, K.; Bhattacharya, R.; Smith, M. C.; Villaluenga, I.; Newman, J.; Balsara, N. P. Negative Transference Numbers in Poly(ethylene oxide)-Based Electrolytes. *J. Electrochem. Soc.* **2017**, *164*, E3569–E3575.
(8) Ma, Y.; Doyle, M.; Fuller, T. F.; Doeff, M. M.; De Jonghe, L. C.; Newman, J. The Measurement of a Complete Set of Transport Properties for a Concentrated Solid Polymer Electrolyte Solution. *J Electrochem Soc* **1995**, *142*, 1859–1868.
(9) Pozyczka, K.; Marzantowicz, M.; Dygas, J. R.; Krok, F. Ionic Conductivity and Lithium Transference Number of Poly(ethylene oxide):LiTFSI System. *Electrochim. Acta* **2017**, *227*, 127–135.
(10) Schauser, N. S.; Sanoja, G. E.; Bartels, J. M.; Jain, S. K.; Hu, J. G.; Han, S.; Walker, L. M.; Helgeson, M. E.; Seshadri, R.; Segalman, R. A. Decoupling Bulk Mechanics and Mono- and Multivalent Ion Transport in Polymers Based on Metal-Ligand Coordination. *Chem. Mater.* **2018**, *30*, 5759–5769.
(11) Mindemark, J.; Lacey, M. J.; Bowden, T.; Brandell, D. Beyond PEO—Alternative Host Materials for Li+-Conducting Solid Polymer Electrolytes. *Prog. Polym. Sci.* **2018**, *81*, 114–143.
(12) Lai, J.-C.; Jia, X.-Y.; Wang, D.-P.; Deng, Y.-B.; Zheng, P.; Li, C.-H.; Zuo, J.-L.; Bao, Z. Thermodynamically stable whilst kinetically labile coordination bonds lead to strong and tough self-healing polymers. *Nat. Commun.* **2019**, *10*, 1164.
(13) Grindy, S. C.; Lenz, M.; Holten-Andersen, N. Engineering Elasticity and Relaxation Time in Metal-Coordinate Cross-Linked Hydrogels. *Macromolecules* **2016**, *49*, 8306–8312.
(14) Mozhdehi, D.; Ayala, S.; Cromwell, O. R.; Guan, Z. Self-Healing Multiphase Polymers via Dynamic Metal-Ligand Interactions. *J. Am. Chem. Soc.* **2014**, *136*, 16128–16131.
(15) Rao, Y.-L.; Chortos, A.; Pfattner, R.; Lissel, F.; Chiu, Y.-C.; Feig, V.; Xu, J.; Kurosawa, T.; Gu, X.; Wang, C.; He, M.; Chung, J. W.; Bao, Z. Stretchable Self-Healing Polymeric Dielectrics Cross-Linked Through Metal-Ligand Coordination. **2016**,
(16) Schauser, N. S.; Grzetic, D. J.; Tabassum, T.; Kliegle, G. A.; Le, M. L.; Susca, E. M.; Antoine, S.; Keller, T. J.; Delaney, K. T.; Han, S.; Seshadri, R.; Fredrickson, G. H.; Segalman, R. A. The Role of Backbone Polarity on Aggregation and Conduction of Ions in Polymer Electrolytes. *J. Am. Chem. Soc* **2020**, *142*, 7055–7065.
(17) Sanoja, G. E.; Schauser, N. S.; Bartels, J. M.; Evans, C. M.; Helgeson, M. E.; Seshadri, R.; Segalman, R. A. Ion Transport in Dynamic Polymer Networks Based on Metal–Ligand Coordination: Effect of Cross-Linker Concentration. *Macromolecules* **2018**, *51*, 2017–2026.
(18) Fenton, D. E.; Parker, J. M.; Wright, P. V. Complexes of Alkali Metal Ions with Poly(ethylene Oxide). *Polymer* **1973**, *14*, 589.
(19) Ratner, M. A.; Shriver, D. F. Ion Transport in Solvent-Free Polymers. *Chem. Rev* **1988**, *88*, 109–124.
(20) Bocharova, V.; Sokolov, A. P. Perspectives for Polymer Electrolytes: A View from Fundamentals of Ionic Conductivity. *Macromolecules* **2020**,
(21) Savoie, B. M.; Webb, M. A.; Miller, T. F. Enhancing Cation Diffusion and Suppressing Anion Diffusion via Lewis-Acidic Polymer Electrolytes. *J. Phys. Chem. Lett.* **2017**, *8*, 641–646.
(22) Borodin, O.; Smith, G. D. Li+ Transport Mechanism in Oligo(Ethylene Oxide)s Compared to Carbonates. *J Solut. Chem* **2007**, *36*, 803–813.
(23) Mongcopa, K. S. I.; Tyagi, M.; Mailoa, J. P.; Samsonidze, G.; Kozinsky, B.; Mullin, S. A.; Gribble, D. A.; Watanabe, H.; Balsara, N. P. Relationship between Segmental Dynamics Measured by Quasi-Elastic Neutron Scattering and Conductivity in Polymer Electrolytes. *ACS Macro Lett.* **2018**, *7*, 504–508.
(24) Wang, Y.; Fan, F.; Agapov, A. L.; Saito, T.; Yang, J.; Yu, X.; Hong, K.; Mays, J.; Sokolov, A. P. Examination of the fundamental relation between ionic transport and segmental relaxation in polymer electrolytes. *Polymer* **2014**, *55*, 4067–4076.

Graphical TOC Entry

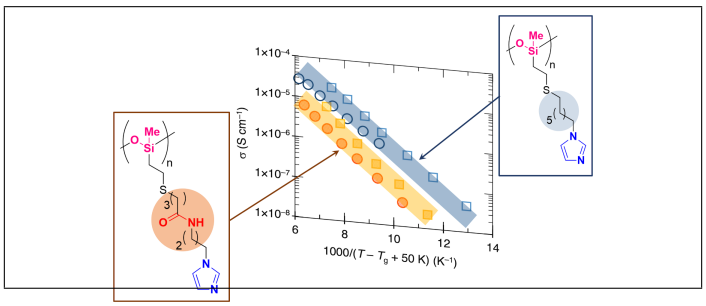

Supporting information for:

The Glass Transition Temperature and Ion Binding Determine Conductivity and Lithium–Ion Transport in Polymer Electrolytes

Nicole S. Schauser, Andrei Nikolaev, Peter M. Richardson, Shuyi Xie, Keith Johnson, Ethan M. Susca, Hengbin Wang, Ram Seshadri, Raphaële J. Clément, Javier Read de Alaniz, and Rachel A. Segalman

Materials Department, Materials Research Laboratory,
Mitsubishi Chemical Center for Advanced Materials,
Department of Chemistry and Biochemistry, and *Department of Chemical Engineering*
University of California, Santa Barbara, California 93106, United States

E-mail: segalman@ucsb.edu

Experimental:

PVMS synthesis: Two batches of poly(vinyl methyl siloxane) (PVMS) were synthesized by anionic polymerization using standard Schlenk line techniques. For the first, 200 mL of uninhibited and dry THF was further purified by distillation over n-butyl lithium and dried by the addition of 260 µL of sec-butyl lithium at 0 °C, after which the solution was allowed to warm to room temperature. The monomer, 1,3,5-trivinyl-1,3,5-trimethyl-cyclotrisiloxane (Gelest), was degassed by four freeze-pump-thaw cycles and used without additional purification. 260 µL of sec-butyl lithium was added to THF at 0 °C as initiator, followed by the addition of 15.5 mL of degassed monomer. The reaction was allowed to proceed for 10 min at 0 °C before termination with degassed methanol. The solution was concentrated and precipitated in methanol three times. The second batch followed a similar synthesis procedure, but with 50 mL of THF dried with the addition of 400 µL sec-butyl lithium. 8.5 mL degassed monomer was initiated with 75 µL n-butyl lithium. The reaction was allowed to proceed for 3 h at 0 °C before termination with degassed methanol. The polymer was purified through three precipitations in water, a 2 day dialysis in THF, and filtering through a PTFE plug. Size exclusion chromatography (SEC) was performed on a Waters Alliance HPLC instrument using a refractive index detector and Agilent PLgel 5 µm MiniMIX-D column at 35 °C with THF as the eluent. Dispersity index (Đ) was determined against polystyrene calibration standards (Agilent Technologies). The PVMS molecular weight was estimated from SEC using Polystyrene standards.

Carbon-linked imidazole synthesis.

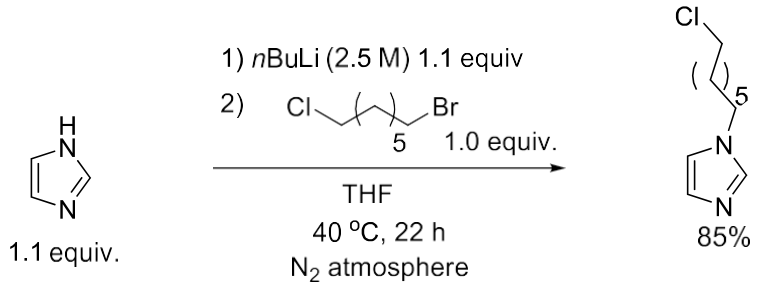

To an oven dried round bottom flask equipped with a magnetic stir bar, imidazole (1.1 equiv.) and half the total volume of THF was added 1.1 equiv. of 2.5 M *n*BuLi in hexane at ambient temperature. This solution was stirred for 30 minutes at ambient temperature under dinitrogen atmosphere. To this reaction was added a solution of 1-bromo-7-chloroheptane in THF to a final concentration of 0.3 M in imidazole. This reaction mixture was placed in an oil bath preheated to 40 ˚C and stirred for 22 hours. Upon completion, the reaction was filtered through a pad of silica and concentrated *in vacuo*. The 1-(7-chloroheptyl)-1*H*-imidazole was isolated in 85% yield and used for the next step without further purification. The ^{1}H-NMR data matched that of previously reported structure.[1]

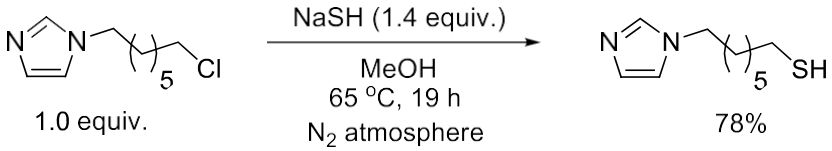

To an oven dried round bottom flask equipped with a magnetic stir bar was added NaSH (1.4 equiv.) followed by a 0.35 M solution of 1-(7-chloroheptyl)-1*H*-imidazole in deoxygenated absolute MeOH at ambient temperature. This reaction mixture was placed in an oil bath preheated to 65 ˚C and stirred for 19 hours. Upon completion, the reaction was filtered through a pad of silica and concentrated *in vacuo*. The 7-(1*H*-imidazol-1-yl)heptane-1-thiol was isolated in 78% yield and used for the next step without further purification.

Polymer functionalization.

Amide-containing PMS-6-Amide-3-Im. N-(2-(1H-Imidazol-1-yl)propyl)-4-mercaptobutanamide (Im-SH) was synthesized as previously reported by Sanoja et al.[2] Dried PVMS was weighed out and dissolved in THF. An appropriate mass of Im-SH was dissolved in methanol and added to the flask to achieve a thiol to vinyl ratio of 1.75:1. DMPA (2,2-Dimethoxy-2-phenylacetophenone) was added as an initiator to vinyl ratio of 0.2:1. The final methanol/THF solvent ratio was adjusted to be 20/80 to maintain solubility during reaction, with a 0.1 M PVMS concentration. The reaction was degassed

with nitrogen for 30 min, after which the reaction was allowed to proceed under UV (365 nm) light for 2 h with continuous stirring. The polymer was purified by precipitation in acetonitrile, then dried *in vacuo* at 55 °C in the presence of phosphorous pentoxide and immediately transferred to a nitrogen glove box.

Amide-free PMS-10-Im. To an oven dried round bottom flask equipped with a magnetic stir bar was added 7-(1*H*-imidazol-1-yl)heptane-1-thiol (3.0 equiv.), PVMS, DMPA (2,2-dimethoxy-2-phenylacetophenone) (10 mol%) followed by deoxygenated absolute DCM to concertation of 0.1 M in PVMS. This reaction mixture was irradiated with 365 nm light for 20 hours. Upon completion, the crude mixture was concentrated *in vacuo*. The polymer was purified by precipitation in THF, then dried under high vacuum and immediately transferred to a nitrogen filled glove box.

Salt addition. Polymers were weighed into 7 mL vials and dissolved in anhydrous methanol inside a nitrogen glove box. Stock solutions of lithium bis(trifluoromethylsulfonyl)imide (LiTFSI, Alfa Aesar) ranging from 0.1 M to 1 M were prepared using anhydrous methanol. Appropriate volumes of LiTFSI stock solution were added to each polymer vial to achieve nominal molar ratios of Li^+ to imidazole of 0.03, 0.1, or 0.3. The sample vials were sealed, removed from the glovebox and frozen in LN_2 before being opened and quickly transferred to a vacuum oven and dried *in vacuo* (1×10^{-3} Torr) at room temperature overnight, and then at 60 °C to 90 °C for 24 h. The samples were then transferred to a high vacuum oven (3×10^{-8} Torr) at 60 °C for 24 h to ensure complete removal of solvent. Finally, the samples were transferred into a nitrogen glove box for storage and measurement.

Conductivity measurements. Total ionic conductivity was measured as a function of temperature on samples sandwiched between parallel ITO blocking electrodes using electrochemical impedance spectroscopy (EIS). The ITO-coated glass electrodes (Thin Film Devices) were cleaned by sonication for 5 min each in detergent, DI water, acetone and isopropyl alcohol, followed by a 5 min UV/ozone treatment (Jelight Company Inc., Model 18). The electrode thicknesses were measured using a micrometer, after which a double-sided Kapton tape spacer with a 1/8" hole was added to one electrode. Polymer samples were loaded into the hole in the Kapton spacer in a nitrogen filled glove box. Samples were heated to about 30 °C above their T_g before being sealed with a second ITO electrode. All samples were then heated to 110 °C and pressed in a hand press. The final stack thickness was measured using a micrometer, and the sample thickness was determined by subtracting the electrode thicknesses. EIS was measured with a Biologic SP-200 potentiostat using a sinusoidal 100 mV signal from 1 MHz to 1 Hz at temperatures ranging from 30 °C to 110 °C. The data was converted into dielectric storage and loss, and the ionic conductivities determined from the real component of conductivity at the maximum in

tan(δ).[3] Three samples were measured for each composition, and the average and standard deviation are reported in the manuscript.

Thermal characterization. Aluminum DSC pans were loaded with polymer samples in a nitrogen filled glove box and briefly exposed to air during sealing of the pans. The glass transition temperature (T_g) of each sample was measured using a Perkin Elmer DSC 8000 on second heating at 20 °C min^{-1} at the midpoint of the step transition. The T_g of PMS-10-Im without salt addition was measured on a TA Instruments Q2000 DSC.

NMR. All ^{7}Li and ^{19}F solid-state NMR experiments were performed on either a 4 mm double resonance (HX) magic angle spinning (MAS) probe or a Diff50 probe fitted with either a 10 mm ^{19}F or ^{7}Li coil. All measurements were done on a 300 MHz (7.05 T) SWB Bruker NMR spectrometer. The polymer samples were packed into 4 mm MAS rotors by adding small amounts of polymer and centrifuging the sample down at 10 kHz for around 2 min each time, until the rotor was full. The rotor was packed inside a nitrogen or argon filled glovebox. The packed NMR rotor was then either used directly inside the 4 mm MAS probe or placed inside a 5 mm NMR tube equipped with a valve which kept an inert atmosphere around the sample. In both instances the sample was then temperature controlled by a flow of N_2 gas at a rate of 800 L hr^{-1} which ensured an inert atmosphere. The temperature for each probe was calibrated using dry methanol and dry ethylene glycol at sub-ambient and elevated temperatures, respectively.

The power level used for the ^{7}Li on the Diff50 probe was 100 W with a 90° pulse duration of around 16 μs (15.6 kHz). The power level used for the ^{7}Li on the 4 mm MAS probe was 100 W with a 90° pulse duration of around 3 μs (83.3 kHz). The power level used for the ^{19}F insert on the Diff50 probe was 50 W with a 90° pulse duration of around 11 μs (23.4 kHz). For all measurements, a recycle delay of around 5 T_1 was applied before each scan when signal averaging, to allow full relaxation. The ^{7}Li chemical shift was calibrated using a 1 M LiCl aqueous solution (single peak at 0 ppm) while the ^{19}F chemical shift was referenced against a neat PF_6 sample exhibiting a doublet centered around 71.7 ppm.

The $T_{1\rho}$ experiments were measured by applying a spin-locking pulse during evolution of the spins following an initial 90° excitation pulse. The spin-locking frequency chosen here was 10 kHz for all samples. The PFG-NMR experiments used a diffusion sequence which includes a stimulated echo to protect the signal from T_2 relaxation, which is typically very short in these polymer systems. The diffusion was measured using a variable magnetic field gradient strength sequence, where the maximum gradient available was 2800 G cm^{-1}. The selection of gradient strength, along with the gradient duration (δ) and diffusion time (Δ) were chosen for each measurement to ensure an appropriate window on the decay curve was acquired. The value of δ and diffusion time Δ never exceeded 10 ms and 100 ms respectively and were kept as low as possible while using the strongest gradient strength possible in order to achieve the greatest possible signal to noise.

Additional SI details:

Polymer SEC:

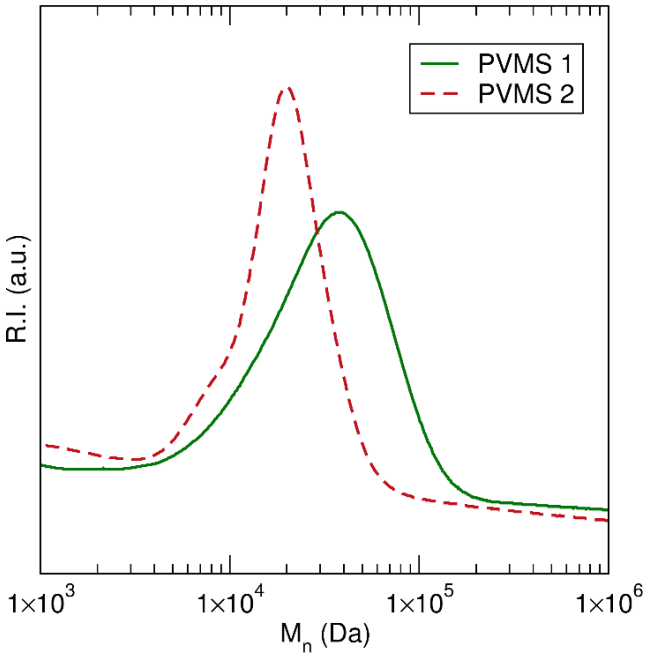

Figure S1. Polymer SEC traces.

Table S1. SEC characterization for the polymer backbones used in this study. M_n and Đ are calculated against polystyrene standards. We note the difference in molecular weight between the two polymer backbones is not likely to cause significant changes in conductivity or transference, as previously shown for poly(ethylene oxide) electrolytes.[4]

Polymer backbone	Used for samples	M_n of backbone (kDa)	Đ
PVMS 1	PMS-6-Amide-3-Im	29	1.60
PVMS 2	PMS-10-Im	19	1.29

Solution-state NMRs:

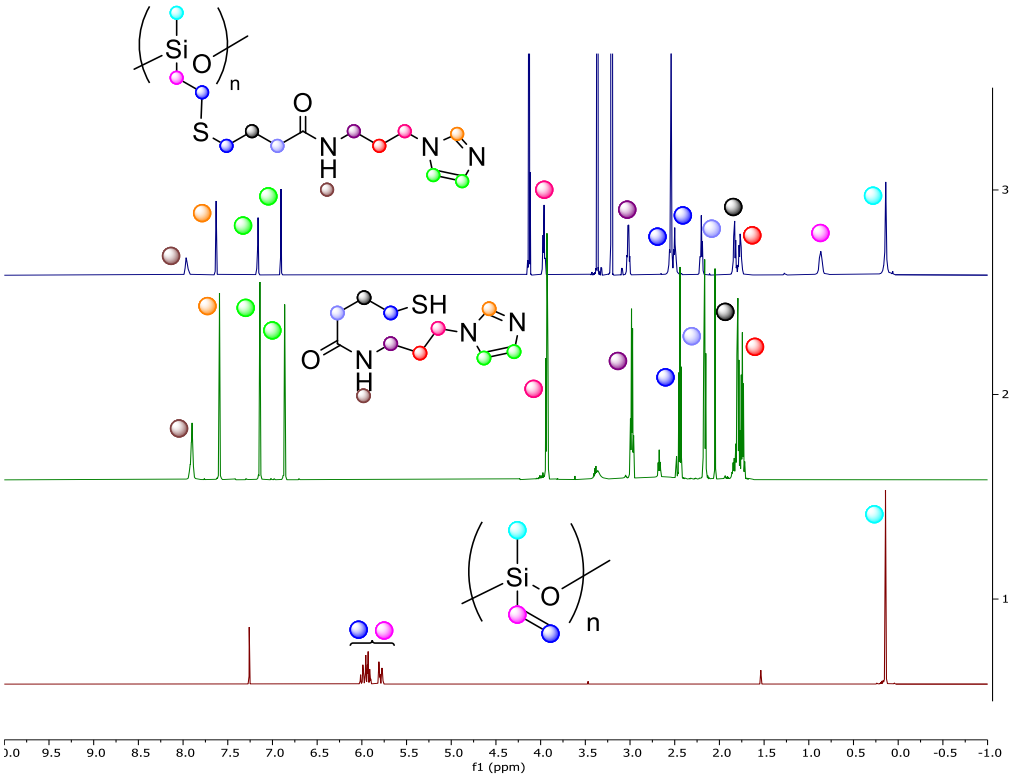

Figure S2. NMR of PVMS, amide-containing imidazole thiol (ImSH) and PMS-6-Amide-3-Im functionalized polymer in $CDCl_3$, $CDCl_3$ and DMSO-d6, respectively.

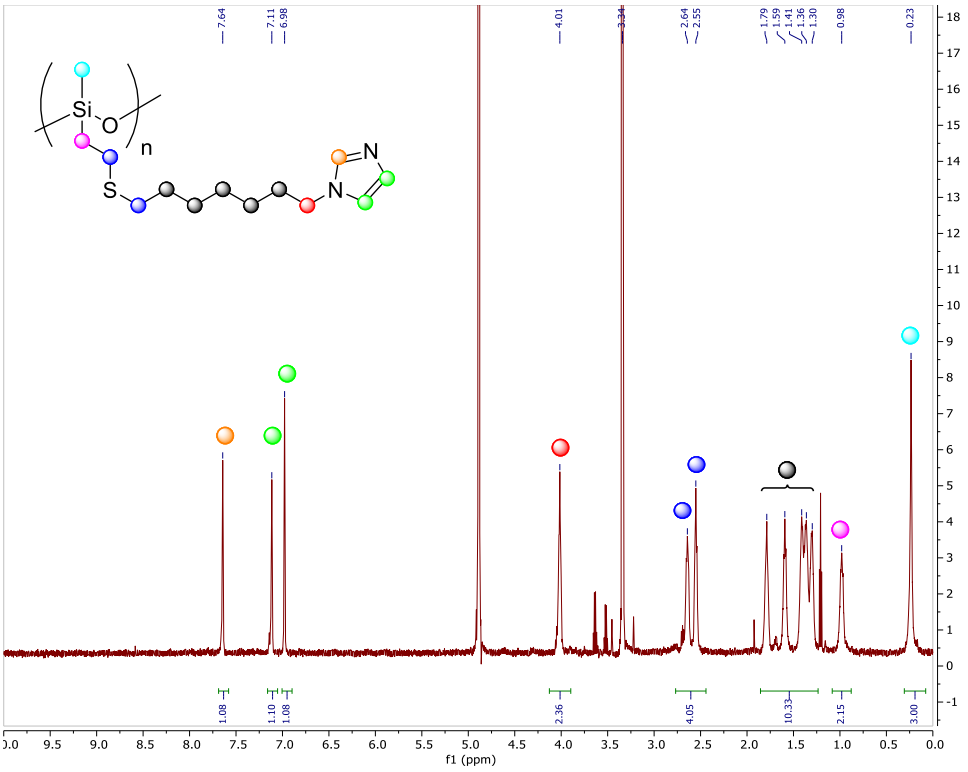

Figure S3. ^{1}H(600 MHz, CD_3OD)-NMR spectrum of *Amide-free PMS-10-Im*.

DSC curves:

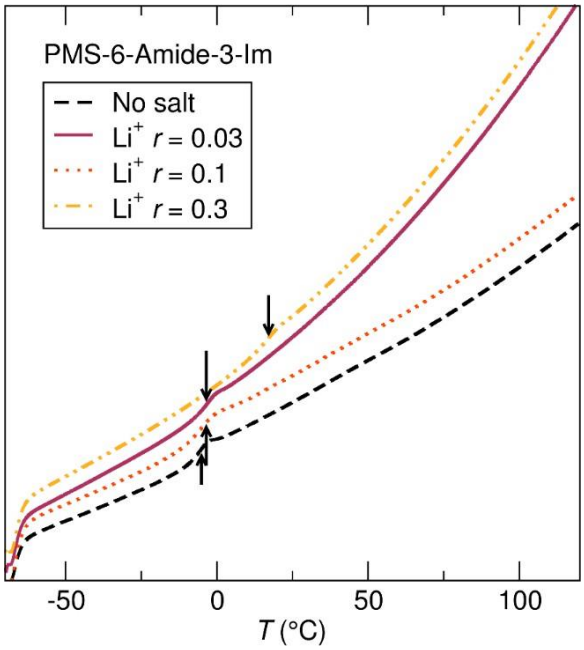

Figure S4. PMS-6-Amide-3-Im DSC traces showing T_g transitions and no crystallinity. Taken on second heating at 20 °C min^{-1}.

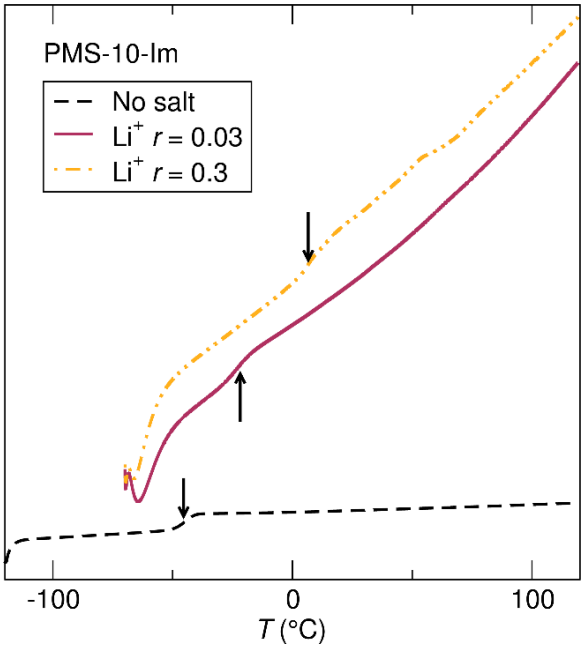

Figure S5. PMS-10-Im DSC traces showing T_g transitions and no crystallinity. Taken on second heating at 20 °C min^{-1}. The T_g of the polymer with r = 0.1 salt concentration was not measured.

Table S2. T_g values for polymer samples of this study, with and without LiTFSI salt addition.

Polymer	T_g no salt (°C)	T_g r = 0.03 (°C)	T_g r = 0.1 (°C)	T_g r = 0.3 (°C)
PMS-6-Amide-3-Im	– 8	– 6	– 7	13
PMS-10-Im	– 44	– 22		7

Ionic Conductivity.

Table S3. Ionic conductivity in S cm^{-1} with standard deviation in parentheses tabulated as a function of temperature.

Sample	30 °C	40 °C	50 °C	60 °C	70 °C	80 °C	90 °C
PMS-6-Amide-3-Im r = 0.03	1.02×10^{-8} (2.4×10^{-9})	4.63×10^{-8} (1.1×10^{-8})	1.65×10^{-7} (4.1×10^{-8})	4.85×10^{-7} (1.3×10^{-7})	1.23×10^{-6} (3.6×10^{-7})	2.76×10^{-6} (8.8×10^{-7})	5.61×10^{-6} (1.9×10^{-6})
PMS-6-Amide-3-Im r = 0.1	1.12×10^{-8} (1.3×10^{-9})	5.45×10^{-8} (2.1×10^{-9})	2.03×10^{-7} (3.8×10^{-9})	6.19×10^{-7} (3.1×10^{-8})	1.61×10^{-6} (1.2×10^{-7})	3.67×10^{-6} (3.5×10^{-7})	7.55×10^{-6} (8.5×10^{-7})
PMS-6-Amide-3-Im r = 0.3			1.27×10^{-8} (5.0×10^{-9})	6.21×10^{-8} (1.8×10^{-8})	2.45×10^{-7} (4.6×10^{-8})	8.10×10^{-7} (7.9×10^{-8})	2.34×10^{-6} (2.2×10^{-7})
PMS-10-Im r = 0.03	6.47×10^{-7} (3.2×10^{-8})	1.51×10^{-6} (9.4×10^{-8})	3.14×10^{-6} (2.3×10^{-7})	5.90×10^{-6} (4.8×10^{-7})	1.02×10^{-5} (9.0×10^{-7})	1.66×10^{-5} (1.5×10^{-6})	2.55×10^{-5} (2.5×10^{-6})
PMS-10-Im r = 0.1	6.29×10^{-7} (4.8×10^{-8})	1.71×10^{-6} (1.4×10^{-7})	4.1×10^{-6} (3.3×10^{-7})	8.83×10^{-6} (6.9×10^{-7})	1.74×10^{-5} (1.3×10^{-6})	3.19×10^{-5} (2.1×10^{-6})	5.5×10^{-5} (3.2×10^{-6})
PMS-10-Im r = 0.3	1.81×10^{-8} (9×10^{-10})	1.01×10^{-7} (1.2×10^{-8})	4.05×10^{-7} (6.5×10^{-8})	1.29×10^{-6} (2.4×10^{-7})	3.40×10^{-6} (6.5×10^{-7})	7.79×10^{-6} (1.5×10^{-6})	1.59×10^{-5} (3×10^{-6})

Conductivity data can also be normalized in a Tg/T fashion instead of the VFT normalization used in Figure 3. This is shown in Figure S6, where it can be seen that the conductivity gains for the amide-free polymer remain similar to those seen in Figure 3. Conductivity gains reduce at higher temperatures farther removed from Tg.

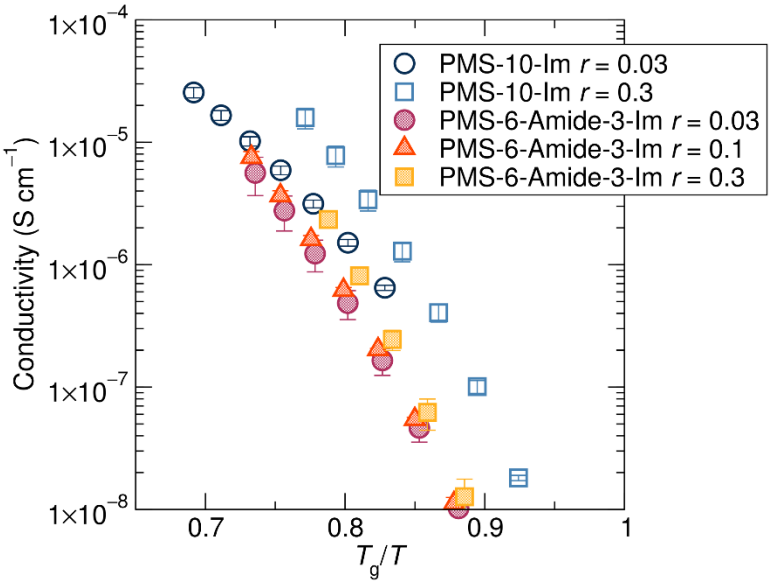

Figure S6. Ionic conductivity performance normalized by Tg in a Tg/T fashion still shows the improvements in the conductivity performance of the polymer without amide functionality (PMS-10-Im) compared to that with amide (PMS-6-Amide-3-Im).

Solid-state NMR:

Diffusion

PFG-NMR was measured for the 0.1 Li:Monomer amide-free polymer as well as the 0.3 Li:Monomer polymer. The 0.1 salt concentration sample showed some evidence of having a crosslinked portion of the polymer revealed by NMR, however this did not change the overall conduction level of the polymer. The diffusion data for the 0.1 and 0.3 (also presented in the main text) is displayed in Table S4.

Table S4. Self-diffusion constants for amide-free polymers (r=0.1 and r=0.3) at various temperatures.

r = 0.1	Temp. (K)	D(^{7}Li) (m^2s^{-1})	D(^{19}F) (m^2s^{-1})	t_+ (%)	σ_+ (Scm^{-1})	σ_- (Scm^{-1})	σ_{total} (Scm^{-1})	$\sigma_{measured}$ (Scm^{-1})
	337.1	1.70E-13	2.29E-13	42.61	1.99E-06	2.68E-06	4.67E-06	
	345.8	2.84E-13	3.98E-13	41.64	3.24E-06	4.54E-06	7.77E-06	
	354.6	4.97E-13	6.58E-13	43.03	5.52E-06	7.31E-06	1.28E-05	
r = 0.3	Temp. (K)	D(^{7}Li) (m^2s^{-1})	D(^{19}F) (m^2s^{-1})	t_+ (%)	σ_+ (Scm^{-1})	σ_- (Scm^{-1})	σ_{total} (Scm^{-1})	$\sigma_{measured}$ (Scm^{-1})
	345.8	1.68E-13	1.98E-13	45.82	5.73E-06	6.77E-06	1.25E-05	6.05E-06
	354.6	3.06E-13	4.22E-13	42.02	1.02E-05	1.41E-05	2.43E-05	1.17E-05

Figure S7 shows some example diffusion decay curves for both the Li^+ and $TFSI^-$ ions for the 0.3 Li:monomer LiTFSI in the amide-free PVMS polymer. The NMR signal intensity (I) is monitored as a function of gradient strength (G). The signal attenuation can be linked to the diffusion time (Δ), gradient pulse duration (δ) and the self-diffusion constant (D). The diffusion decay curves were all fitted with equation S1.

$$I = I_0 exp\left(-D\gamma^2\delta^2G^2\left(\Delta - \frac{\delta}{3}\right)\right) \qquad (S1)$$

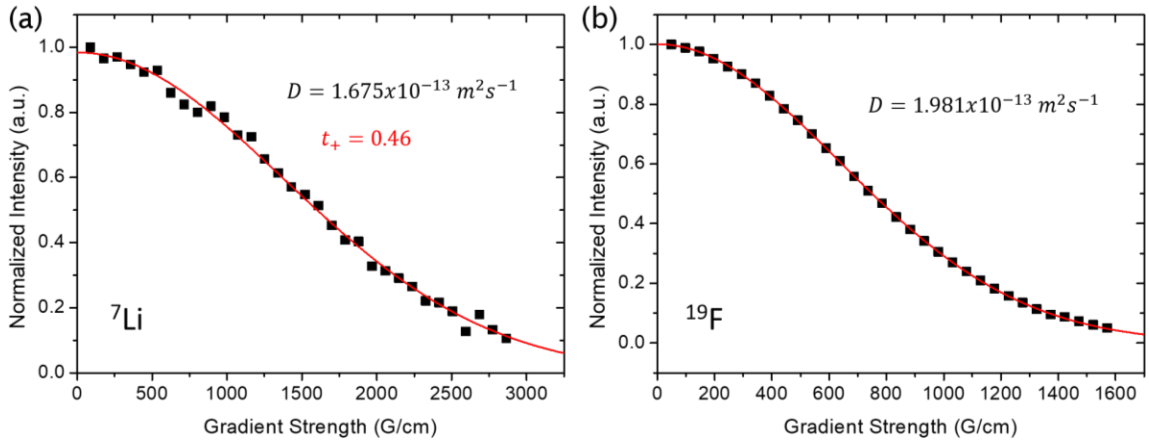

Figure S7 – Example diffusion decay curve from a PFG-NMR experiments on the 0.3 Li:monomer LiTFSI in an amide-free PVMS polymer sample at 72.7 °C for the (a) Li^+ and (b) $TFSI^-$ ions.

$T_{1\rho}$ Relaxation

The $T_{1\rho}$ measurements can give insight into the ion dynamics at lower temperatures than possible via PFG-NMR for these systems. The measurements are a complimentary to the diffusion measurements since they probe a similar timescale. A spin locking frequency of 10 kHz (0.1 ms timescale) was chosen to be on a similar timescale as the diffusion measurements.

For both the amide-containing and amide-free polymers a bi-exponential was required to fit the data. This means there are two distinct locations of the Li^+ ions at all temperatures. Figure S8 shows the temperature dependent $T_{1\rho}$ values for the 0.3 Li:Monomer LiTFSI amide-free PVMS sample.

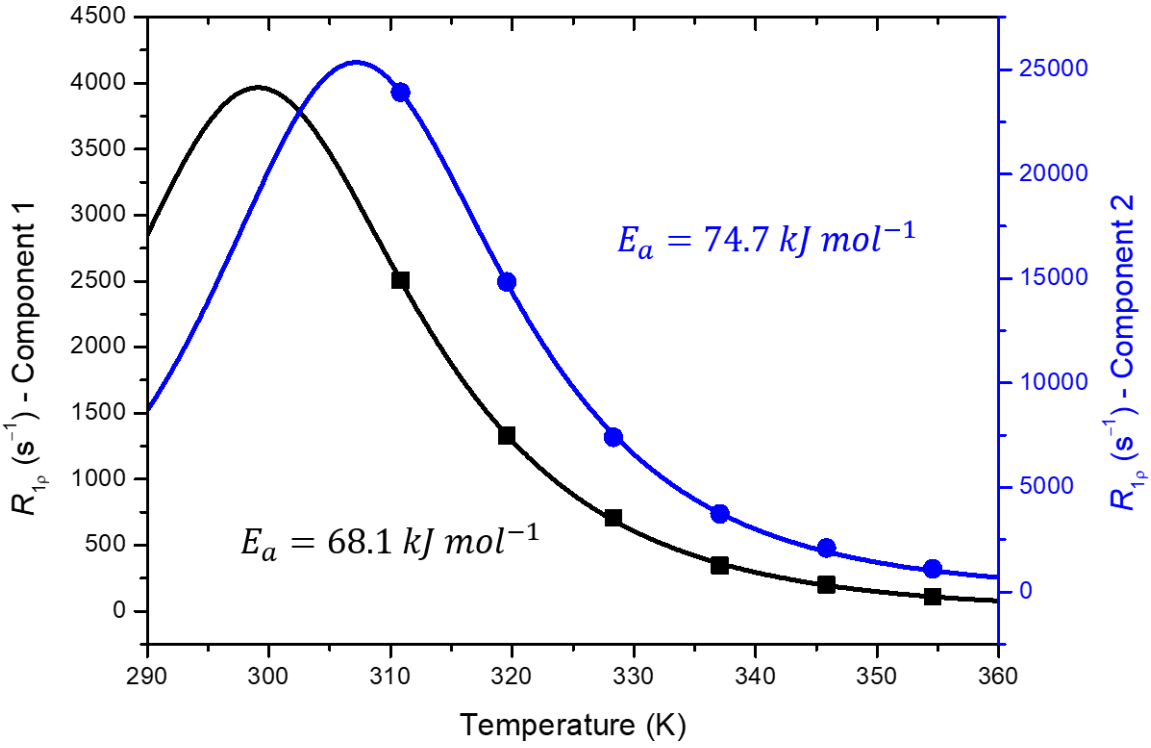

Figure S8. $T_{1\rho}$ values for individual Li^+ components for the 0.3 Li:monomer LiTFSI in an amide-free PVMS polymer sample.

The theoretical equation for $T_{1\rho}$, typically expressed as the relaxation rate ($R_{1\rho,DD} = {}^{1}/_{T_{1\rho,DD}}$), is dependent on the resonant frequency of the nuclei under investigation (ω_0), the spin-locking frequency (ω_1), a pre-exponential factor (k) and a correlation time (τ_c), as shown in equation S2.

$$\frac{1}{T_{1\rho,DD}} = R_{1\rho,DD} = k\left(\frac{3\tau_c}{1+4\omega_1^2\tau_c^2} + \frac{5\tau_c}{1+\omega_0^2\tau_c^2} + \frac{2\tau_c}{1+4\omega_0^2\tau_c^2}\right) \qquad (S2)$$

In equation S2 there is no temperature dependence, however, the correlation time can be expressed in terms of an Arrhenius equation in the form of equation S3.

$$\tau_c = \tau_0 exp\left(-\frac{E_a}{RT}\right) \qquad (S3)$$

where E_a is the activation energy, τ_0 is the pre-exponential factor and R is the universal gas constant. The data in Figure S8 was fitted by combining equations S2 and S3 to extract an activation energy. The activation energies obtained are comparable to that obtained with the diffusion measurements. It is also possible to get the contribution for each of the sites as a function of temperature. Figure S9 shows the data for the 0.3 Li:monomer LiFTSI

amide-free PVMS sample shows the relative contributions of the two sites as a function of temperature. Component 1, which represents the more mobile ('free') Li component, decreases with increasing temperature. Similar effects have been previously seen in salt-doped PEO electrolytes, and have been attributed to increases in ion pairing at higher temperatures.[5]

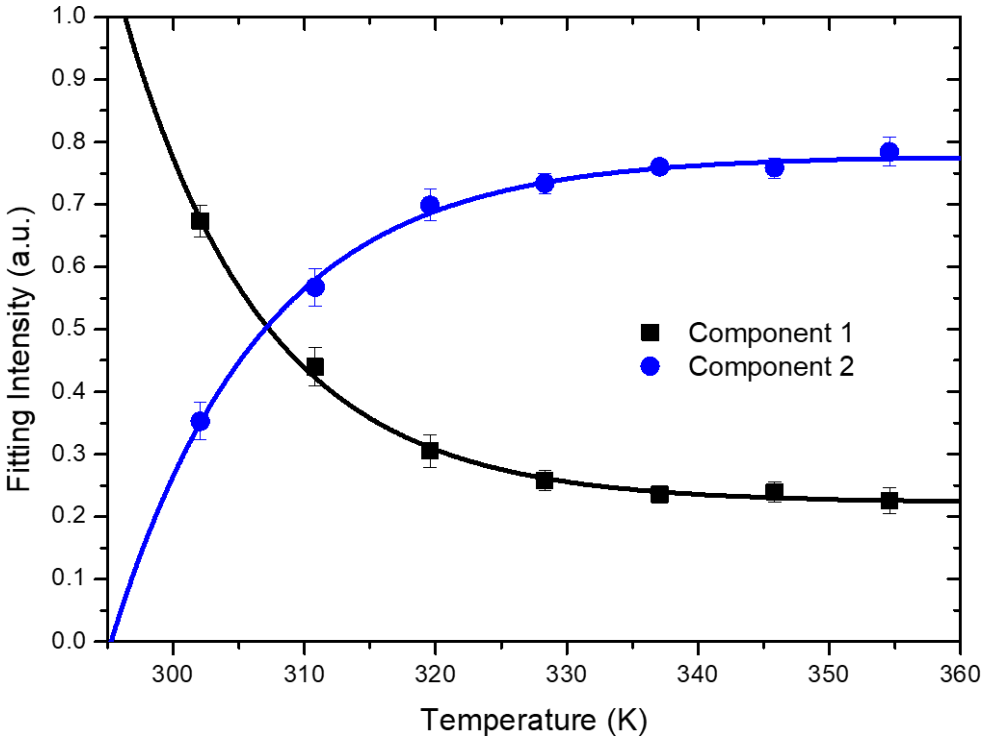

Figure S9. $T_{1\rho}$ fitting intensity values for individual Li^+ components for the 0.3 Li:monomer LiTFSI in an amide-free PVMS polymer sample.

The amide-containing polymer also contains two different lithium sites, exposed via the use of $T_{1\rho}$ measurements. The $T_{1\rho}$ temperature dependence for the 0.1 Li:monomer LiTFSI amide-containing PVMS polymer are shown in Figure S10. The activation energies obtained for the two components are $118 \pm 11\ kJ\ mol^{-1}$ and $94 \pm 10\ kJ\ mol^{-1}$. The two components exhibit higher activation energies than the corresponding amide-free polymer. Since this is attributed to the activation of ion hopping, it is expected that ions with impeded dynamics would exhibit higher activation energies.

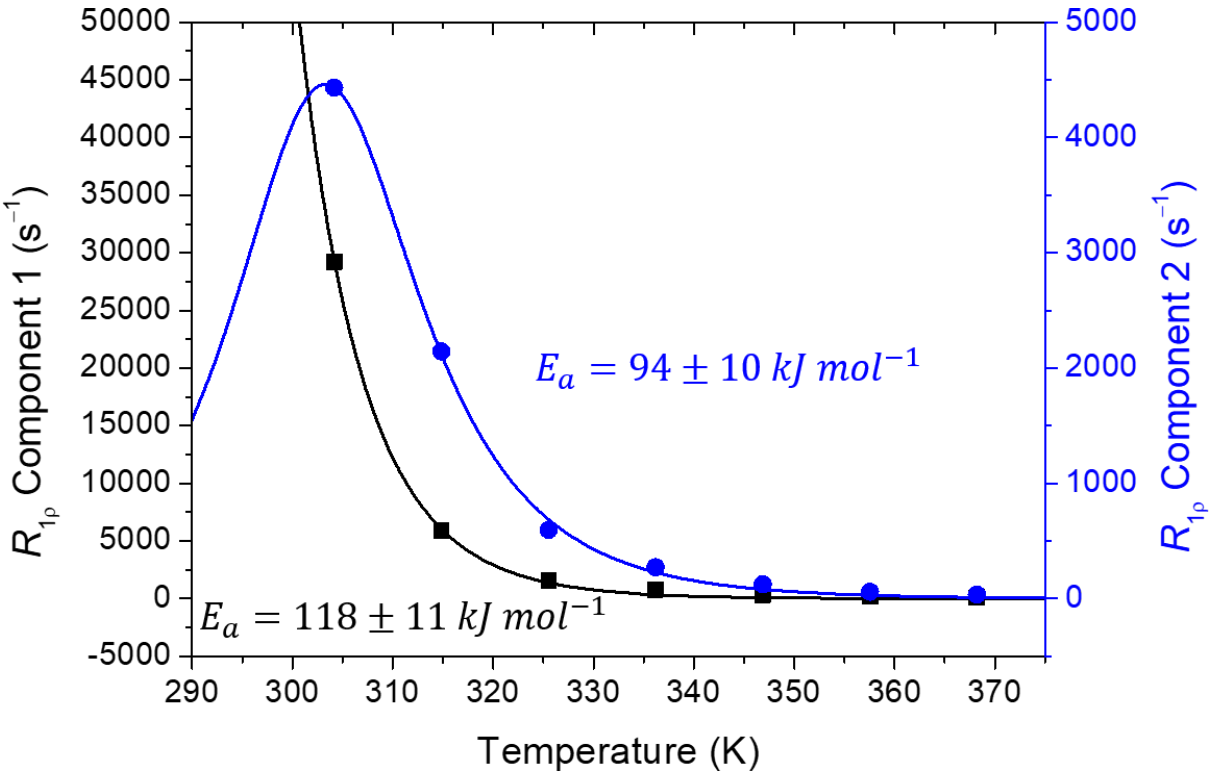

Figure S10. $T_{1\rho}$ values for individual Li^+ components for the 0.1 Li:monomer LiTFSI in an amide-containing PVMS polymer sample.

Ideal Conductivity Calculations

The Nernst-Einstein equation (Equation S4) links the ionic conductivity (σ) to the self-diffusion constants of the anion (D_+) and cation (D_-) if the salt concentration (C) and valency (z_+ and z_-) of the system are known.

$$\sigma = \frac{N_a e^2 C}{k_B T}(z_+{}^2 D_+ + z_-{}^2 D_-) \qquad (S4)$$

Where e is the electron charge, k_B is the Boltzmann constant and T is the absolute temperature of the sample. The valency of LiTFSI is $z_+ = z_- = 1$ and therefore can be simplified in the form of equation S5 for this system.

$$\sigma = \frac{N_a e^2 C}{k_B T}(D_+ + D_-) \qquad (S5)$$

References

(1) Iizuka, K.; Akahane, K.; Momoee, D.; Nakazawa, M.; Tanouchi, T.; Kawamura, M.; Ohyama, I.; Kajiwara, I.; Iguchi, Y.; Okada, T.; et al. *Highly Selective Inhibitors of Thromboxane Synthetase. 1. Imidazole Derivatives*; Pharmaceutical Co., Ltd, 1981; Vol. 24.

(2) Sanoja, G. E.; Schauser, N. S.; Bartels, J. M.; Evans, C. M.; Helgeson, M. E.; Seshadri, R.; Segalman, R. A. Ion Transport in Dynamic Polymer Networks Based on Metal–Ligand Coordination: Effect of Cross-Linker Concentration. *Macromolecules* **2018**, *51*, 2017–2026.

(3) Runt, J.; Fitzgerald, J. J. *Dielectric Spectroscopy of Polymeric Materials: Fundamentals and Applications.*; American Chemical Society, 1997.

(4) Timachova, K.; Watanabe, H.; Balsara, N. P. Effect of Molecular Weight and Salt Concentration on Ion Transport and the Transference Number in Polymer Electrolytes. *Macromolecules*, **2015**, *48*, 7882-7888.

(5) Stolwijk, N. A.; Wiencierz, M.; Heddier, C.; Kösters, J. What Can We Learn from Ionic Conductivity Measurements in Polymer Electrolytes? A Case Study on Poly(ethylene oxide) (PEO)–NaI and PEO–LiTFSI. *J. Phys. Chem. B,* **2012**, *116*, 3065–3074.